Biliverdin inhibits Toll-like receptor-4 (TLR4) expression through nitric oxide-dependent nuclear translocation of biliverdin reductase

Barbara Wegiel[a], David Gallo[a], Eva Csizmadia[a], Thierry Roger[b], Elzbieta Kaczmarek[c], Clair Harris[a], Brian S. Zuckerbraun[d], and Leo E. Otterbein[a,1]

[a]Transplant Institute and [c]Center for Vascular Biology Research, Department of Surgery, Beth Israel Deaconess Medical Center, Harvard Medical School, Boston, MA 02215; [b]Department of Medicine, Infectious Diseases Services, CH-1011 Lausanne, Switzerland; and [d]Department of Surgery, University of Pittsburgh School of Medicine, Pittsburgh, PA 15213

Edited by Solomon H. Snyder, The Johns Hopkins University School of Medicine, Baltimore, MD, and approved October 5, 2011 (received for review June 28, 2011)

The cellular response to an inflammatory stressor requires a proinflammatory cellular activation followed by a controlled resolution of the response to restore homeostasis. We hypothesized that biliverdin reductase (BVR) by binding biliverdin (BV) quells the cellular response to endotoxin-induced inflammation through phosphorylation of endothelial nitric oxide synthase (eNOS). The generated NO, in turn, nitrosylates BVR, leading to nuclear translocation where BVR binds to the Toll-like receptor-4 (TLR4) promoter at the Ap-1 sites to block transcription. We show in macrophages that BV-induced eNOS phosphorylation (Ser-1177) and NO production are mediated in part by Ca^{2+}/calmodulin-dependent kinase kinase. Furthermore, we show that BVR is S-nitrosylated on one of three cysteines and that this posttranslational modification is required for BVR-mediated signaling. BV-induced nuclear translocation of BVR and inhibition of TLR4 expression is lost in macrophages derived from *Enos*$^{-/-}$ mice. In vivo in mice, BV provides protection from acute liver damage and is dependent on the availability of NO. Collectively, we elucidate a mechanism for BVR in regulating the inflammatory response to endotoxin that requires eNOS-derived NO and TLR4 signaling in macrophages.

heme oxygenase | innate immunity | bile pigments

Biliverdin (BV) and *biliverdin reductase* (BVR) are a part of a well-characterized signaling cascade and the only metabolic pathway that leads to the generation of bilirubin (BR) (1–4). Recently, we defined a role and cellular localization for BVR and documented its localization as present on the external cell surface of macrophages (Mϕ) (referred to as BVR_{surf}) that explains, in part, the potent antiinflammatory effects that have been ascribed to BV by others and us (5–7). The conversion of BV to BR by BVR is a physiological process that occurs continuously by the cell as a component of heme catalysis, and in pathological conditions, it can reach >50 μM (8–11). In vivo in mice, BV is rapidly converted to BR within minutes after its endogenous administration, primarily through BVR_{surf}. BVR, akin to heme oxygenase (HO), is critical in appropriate heme metabolism, but both BVR and HO possess powerful alternative modes of action as cytoprotective homeostatic molecules (2). BVR is incredibly pleiotropic, with defined signaling capabilities (4, 5, 12), zinc finger transcriptional activity (13), and joint interactions with mitogen activated protein kinase (MAPK), mitogen activating extracellular regulated kinase (MEK), protein kinase B (Akt), and protein kinase C (PKC) in response to cell stimulation (4). Phosphorylation of BVR by MEK results in the ternary complex translocating to the nucleus to regulate transcription of HO-1 and other genes (1). BVR translocation to the nucleus in response to endotoxin and heavy metals is dependent on cGMP signaling (14), suggesting that perhaps nitric oxide (NO) could modulate BVR localization. Moreover, BR administration has been shown to induce neuronal NO synthase (nNOS) activation and increase NO generation in neurons, although the mechanism remains unclear (15). Therefore, we hypothesized that there is a collaborative link between BVR and NO.

In addition to binding to heme moieties to initiate signaling, NO can also nitrosylate target proteins to modulate protein function, with endothelial nitric oxide synthase (eNOS) -dependent S-nitrosylation being an innate mechanism by which inhibition of signal transduction can occur. For instance, NO-derived from L-arginine inhibits Toll-like receptor-4/2 (TLR4/2) expression in models of acute lung injury (16, 17), and nitrosylation of caspase-3 inhibits TNF-α–induced apoptosis in hepatocytes (18). We recently reported that BVR_{surf} exerts antiinflammatory effects in Mϕ in response to endotoxin, but the mechanism of action remained unclear (5). We have now expanded these observations in vivo and in vitro and tested the hypothesis that BV-induced phosphorylation of eNOS increases NO generation, which contributes in part to the antiinflammatory capabilities of BVR. S-nitrosylation of BVR directs translocation of BVR to the nucleus, where it binds the TLR4 promoter to regulate the innate inflammatory response.

Results

BV Induces Phosphorylation of eNOS Through Calmodulin-Dependent Kinase Kinase in Mϕ. Previously, we showed that treatment of Mϕ with BV results in a rapid increase in phosphorylation of Akt through a BVR–PI3K-dependent mechanism, leading to up-regulation of IL-10 expression and hepatoprotection (5). Because eNOS activation is known to be downstream of Akt (19) and Ca^{2+}/calmodulin-dependent kinase kinase (CaMMK), we first tested whether BV is present and influences phosphorylation of eNOS in RAW 264.7 Mϕ given that it is a critical regulator of inflammatory responses (Fig. 1*A*) (20). Treatment of RAW 264.7 Mϕ with BV induced phosphorylation of eNOS at Ser-1177 in a time- and dose-dependent fashion (Fig. 1*B* and Fig. S1*A*). A concentration of 50 μM BV was chosen based on previous data showing that this dose induced strong activation of Akt signaling (5). Trypan blue exclusion at 50 μM showed no toxicity of BV through 24 h of incubation (93 ± 3% in BV vs. 96 ± 2% in controls). Moreover, this dose results in the generation of BR in the high/normal range in vivo (21–23). A similar effect of BV on eNOS phosphorylation was also observed in mouse primary Mϕ. The BV-induced increase in eNOS phosphorylation was dependent on BVR, because expression of micro-adapted shRNA-BVR (mirBVR) abrogated the BV-induced increase in phospho-eNOS (Fig. S1*B*). The rapid increase in

Author contributions: B.W., D.G., B.S.Z., and L.E.O. designed research; B.W., D.G., E.C., E.K., C.H., and B.S.Z. performed research; E.C. and T.R. contributed new reagents/analytic tools; B.W. and L.E.O. analyzed data; and B.W., and L.E.O. wrote the paper.

The authors declare no conflict of interest.

This article is a PNAS Direct Submission.

[1]To whom correspondence should be addressed. E-mail: lotterbe@bidmc.harvard.edu.

This article contains supporting information online at www.pnas.org/lookup/suppl/doi:10.1073/pnas.1108571108/-/DCSupplemental.

PHYSIOLOGY

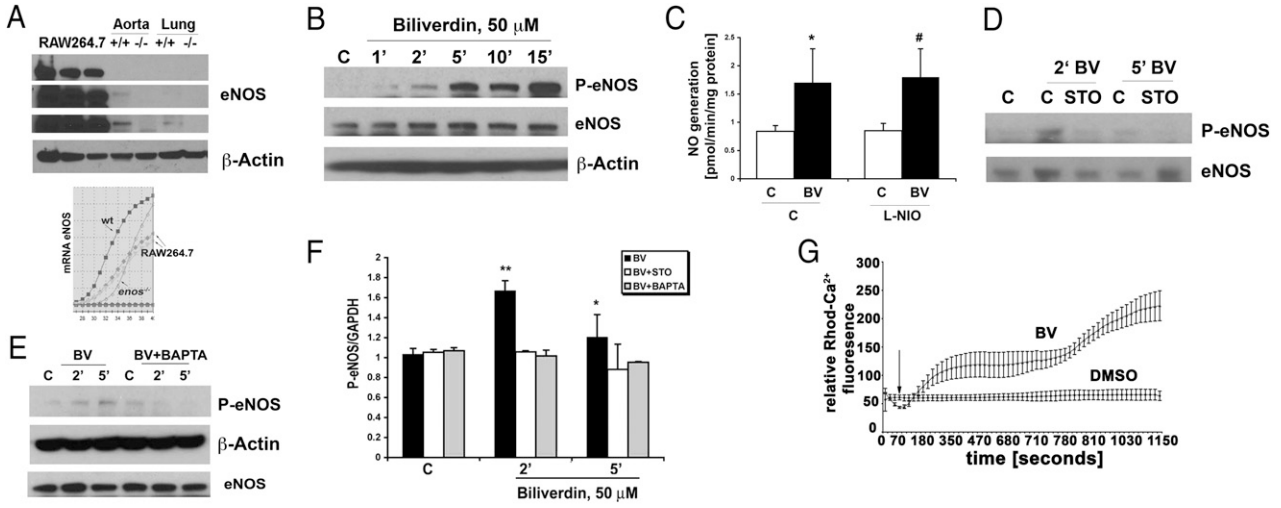

Fig. 1. BV induces phosphorylation of eNOS dependent on Ca^{2+}/CaMKK. (*A*) Representative immunoblot (*Upper*) and PCR profile (*Lower*) with antibodies or primers against eNOS in RAW 264.7 Mϕ and tissues (aorta and lung shown as positive controls) harvested from *Enos*$^{+/+}$ and *Enos*$^{-/-}$ mice. β-Actin was used as a loading control. One of three independent experiments is shown. Different exposure times of the membrane are shown because of differences in the amounts of eNOS present in tissues vs. cells. (*B*) Immunoblot against phosphorylated eNOS (Ser-1177) in RAW 264.7 Mϕ treated with DMSO (C) or biliverdin (BV; 50 μM) over time. eNOS and β-actin were used as loading controls. Data are representative of three independent experiments. (*C*) NO generation was measured in RAW 264.7 Mϕ treated with L-NIO (100 μM) 30 min before BV (50 μM). NO was measured starting 10 min after BV for 30 min. Data represent mean ± SD from three repeated measurements. $P < 0.05$. (*D*) Immunoblot of phospho-eNOS (Ser1177) measured at the indicated times in the presence and absence of the CaMKK inhibitor STO-609 (1 μg/mL) applied to RAW 264.7 Mϕ 1 h before DMSO or BV (50 μM). The blot is representative of three independent experiments. (*E*) Immunoblot of P-eNOS (Ser1177) in RAW 264.7 Mϕ pretreated with the calcium chelator BAPTA for 1 h before addition of BV for the indicated times. Data are representative of three independent experiments. (*F*) Densitometric analyses of P-eNOS/GAPDH of blots in *D* and *E*. Results represent mean ± SD of three independent experiments. *$P < 0.05$ BV5′ vs. control; **$P < 0.01$ BV2′ vs. control. (*G*) Time-lapse studies of calcium influx were measured in RAW 264.7 Mϕ treated with BV (50 μM). Fluorescence intensity was measured every 20 s. Arrow indicates the addition of DMSO or BV. Results represent mean ± SD of two independent experiments.

phosphorylation of eNOS corresponded with concomitant NO production, and this finding was determined to be iNOS-independent, because use of the selective inducible nitric oxide synthase (iNOS) inhibitor, N5-(1-iminoethyl)-L-ornithin, dihydrochloride (L-NIO), had no effect on NO generation in response to BV treatment (Fig. 1*C*). Furthermore, iNOS protein expression was not observed over this early kinetic as expected.

To evaluate whether Akt was involved in the phosphorylation of eNOS in response to BV, we blocked Akt phosphorylation using the selective PI3K inhibitor, LY29004, which had no effect on BV-induced eNOS phosphorylation (Fig. S1*C*). We turned our attention next to MAPK Erk1/2, which has also been shown to be a critical target for BVR (1). In RAW 264.7 Mϕ, inhibition of the MEK-Erk1/2 pathway with the selective inhibitor PD98059 also had no significant effect on eNOS phosphorylation in response to BV (Fig. 1*B* vs. Fig. S1*D*). Because CaMKK is also implicated in eNOS activation, we next blocked this kinase with STO-609, a selective CaMKK inhibitor, which completely abolished BV-induced phosphorylation of eNOS (Fig. 1 *D* and *F*). Given that CaMKK activation is dependent on calcium influx, we next treated RAW 264.7 Mϕ with bis (2-aminophenoxy) ethane tetraacetic acid ester (BAPTA-AM), an intracellular calcium chelator, in the presence or absence of BV, and we observed a significant attenuation of eNOS phosphorylation (Fig. 1 *E* and *F*). To confirm the effects of BV on calcium flux, RAW 264.7 Mϕ were loaded with X-Rhod and then treated with or without BV followed by measurement of fluorescence over time. BV induced a rapid, time-dependent increase in fluorescence vs. vehicle control (Fig. 1*G*).

BVR Is S-Nitrosylated in Mϕ in Response to BV. With the rapid increase in eNOS phosphorylation and known localization of eNOS in the caveolae and the fact that BVR_{surf} is present in the plasma membrane (19), we next tested if BVR signaling was influenced by BV-induced activation of eNOS and NO generation. Rodent BVR has three cysteine residues involved in activity and membrane localization, and therefore, they are potential targets for nitrosylation (5, 24). We hypothesized that S-nitrosylation of one or more of the three cysteines would influence BVR activity and modulate signaling and/or cellular localization of BVR in response to a stimulus. We observed that BVR is S-nitrosylated in response to LPS and to a greater extent, in response to BV (Fig. 2 *A*–*C* and Fig. S2*A*). S-nitrosylation of BVR in response to LPS or BV was assessed by multiple methods: coimmunoprecipitation, NO release from recombinant BVR, and direct NO measurements with an NO analyzer (Figs. 1*C* and 2 *A*–*C* and Fig. S1*E*). Moreover, basal and BV-induced expression of S-nitrosylated BVR is lower in Mϕ isolated from *Enos*$^{-/-}$ vs. elevated in *Enos*$^{+/+}$ mice (Fig. 2*D*), again supporting eNOS as the source of NO that leads to S-nitrosylated BVR. The NO generated in response to LPS is independent of iNOS, because nitrosylation is observed before iNOS expression; also, NO is elevated in the presence of iNOS inhibitor L-NIO (Fig. S1*E*). Furthermore, we show increased S-nitrosylated BVR levels on the cell surface in vivo in the livers of mice injected with LPS (Fig. S2*B*).

S-nitrosylation of enzymes modifies activity (25), and therefore, we next examined whether S-nitrosylation of BVR influenced its activity to convert BV to BR. Addition of BV to RAW 264.7 Mϕ increases BR generation as expected, whereas BV treatment in the presence of the NO donor sodium nitroprusside (SNP) diminished BR generation in both the cytosolic/membrane and nuclear fractions. In contrast, BV treatment in the presence of eNOS inactivated with *N*–amino-L-arginine (L-NAA) accelerated the generation of BR (Fig. S3).

BV Induces NO-Dependent Translocation of BVR to the Nucleus. We next investigated whether the changes in BVR signaling caused by S-nitrosylation affected compartmentalization and localization of BVR. One of the cysteines in BVR_{surf} is located within a prenylation site, and thus, S-nitrosylation of this cysteine might modulate targeting of BVR to the plasma membrane. We hypothesized that negative feedback from eNOS is an endogenous regulatory

mechanism to limit constitutive activation of BVR in the membrane and cytosol.

BV administration led to accumulation of BVR in the nucleus of RAW 264.7 Mϕ and primary bone marrow derived macrophages (BMDM) (Fig. 3*A* and *B* and Fig. S4), which occurred after the BV-induced increase in eNOS phosphorylation and NO generation (Fig. 1). The effect is, in part, dependent on NO generation, because a similar pattern was observed after treatment with the NO donor SNP in the absence of BV, which led to marked accumulation of BVR in the nucleus beginning 1 h after SNP administration (Fig. 3*C*). Pharmacologic inhibition of NO generation with L-NAME resulted in inhibition of BVR translocation to the nucleus (Fig. 3*D*). Finally, nuclear and cytoplasmic BVRs were present in WT BMDM that were treated with BV for 30 min, whereas in *Enos*$^{-/-}$ BMDM, the majority of BVR was expressed in the cytoplasm and/or on the cell surface in response to BV (Fig. S4). These data suggest that BVR translocates to the nucleus in response to BV and in part, requires eNOS-dependent NO generation and S-nitrosylation of BVR.

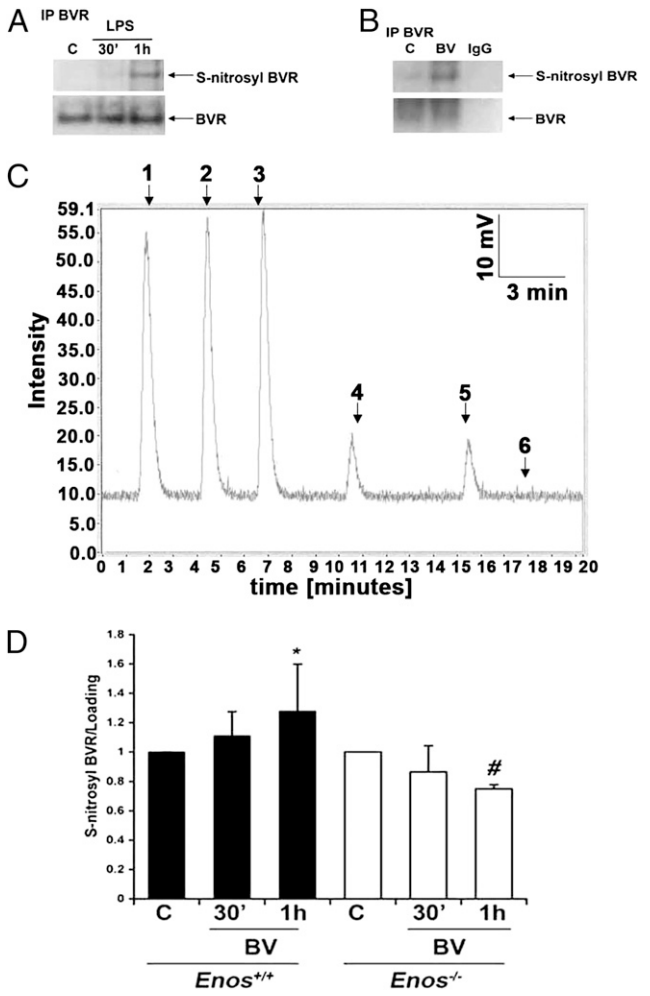

Fig. 2. BVR is S-nitrosylated in response to BV treatment. (*A* and *B*) Representative immunoblots depicting S-nitrosylation measured by using the biotin switch method of BVR in response to 100 ng/mL LPS (*A*) or 50 μM BV for 1 h (*B*). Blots are representative of at least two independent experiments. (*C*) S-nitrosylated cysteine in rat recombinant BVR protein as shown by the NO release method. Peaks 1–3, S-nitrosoglutathione standards; peaks 4 and 5, S-nitrosyl–BVR; peak 6, BVR. Results are representative of three independent experiments. (*D*) Densitometric analyses of three independent coimmunoprecipitation blots for BVR S-nitrosylation. BV-treated bone marrow-derived Mϕ harvested from *Enos*$^{+/+}$ and *Enos*$^{-/-}$ mice showed that BV increases S-nitrosylation of BVR in *Enos*$^{+/+}$ but not *Enos*$^{-/-}$ Mϕ. *$P < 0.04$ vs. control (C); #$P < 0.05$ vs. control (C) as assessed by ANOVA.

Nuclear BVR Blocks Expression of TLR4 and Inflammatory Cytokine Production. BV induces a strong antiinflammatory phenotype in Mϕ in vitro and in vivo, and the effects are dependent, in part, on BVR (either cytosolic or surface-expressed) (5). To investigate potential targets for BV-induced nuclear BVR, we performed a microarray profile on RAW 264.7 cells treated with BV for 4 h and observed a nearly twofold decrease in TLR4 expression vs. controls. We confirmed the effects of BV on TLR4 expression by real-time PCR and observed significant inhibition in TLR4 message in response to BV or an NO donor (Fig. 4*A* and Fig. S5*A*). BV administration blocked TLR4 expression in RAW 264.7 Mϕ, which was reversed by inhibiting NO generation with either L-NAME or L-NAA (Fig. 4*B*). Furthermore, the inhibitory effects of BV on TLR4 expression were lost in BMDM isolated from *Enos*$^{-/-}$ mice (Fig. 4*C*). Using ChIP with antibodies against BVR in the extracts of BV-treated RAW 264.7 Mϕ, we show that BVR binds to the TLR4 promoter in the proximal region spanning −539, which contains GATA and Ap-1 sites (Fig. 4*D*). Mutational analyses of the TLR4 gene showed that TLR4 promoter activity is induced by Ap-1 and repressed by GATA-4 (26). BV treatment blocks TLR4 expression in the absence of GATA-4 (−336 bp) but not Ap-1 (−144 bp). BV had no effect on luciferase activity in both the empty vector as well as the entire promoter construct (−2,715 bp), which exhibited low luciferase activity because of the strong repressive effects of GATA-4 as expected (21–23). These data localized BVR binding to the region spanning −336 bp (Fig. 4*E*). Importantly, the ability of BVR to regulate TLR4 (spanning −336 bp) was lost in cells in which NOS was blocked (Fig. 4*E*). To exclude the unspecific binding of BVR to the TLR4 promoter oligonucleotides, we tested unrelated MMP2 and VEGF promoter oligonucleotides spanning Ap-1 sites as previously described (27) and detect no binding of BVR in these sequences. Furthermore, in the same region of the TLR4 promoter, we were able to pull down interaction of Elk-1 with TLR4, which was slightly inhibited by BV treatment. Additionally, BV administration inhibited TLR4 protein expression in unstimulated RAW 264.7 Mϕ, whereas an NO donor enhanced TLR4 expression (Fig. 5 *A* and *B* and Fig. S5*A*).

Lack of BVR Induces Proinflammatory State of Mϕ. We next investigated the effects of absence of BVR on TLR4 expression. Stable depletion of BVR with selective mirBVR constructs led to enhanced basal expression of TLR4 on the surface of RAW 264.7 Mϕ (Fig. 5*C*), which correlated with a greater than 30-fold

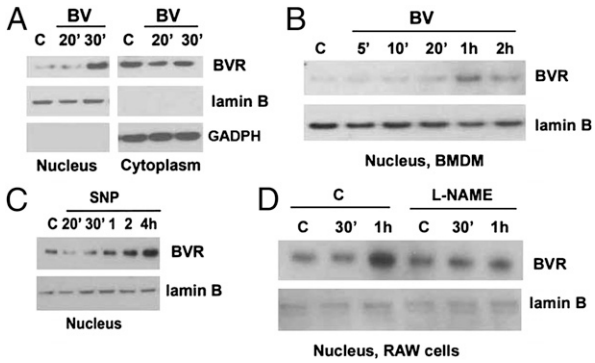

Fig. 3. Nuclear translocation of BVR is dependent on NO generation. (*A–D*) Immunoblots comparing BVR in the nuclear and cytoplasmic fractions of Mϕ treated ± BV (50 μM) ± an NO donor or inhibitor for the indicated time points. (*A*) RAW 264.7 Mϕ. (*B*) BMDM. (*C*) Nuclear BVR in RAW 264.7 Mϕ treated with the NO donor SNAP (100 μM). (*D*) RAW 264.7 Mϕ treated with L-NAME (100 μM) 1 h before BV. Lamin B and GAPDH were used as housekeeping genes for nuclear and cytosolic fractions, respectively. All blots are representative of three independent experiments.

PHYSIOLOGY

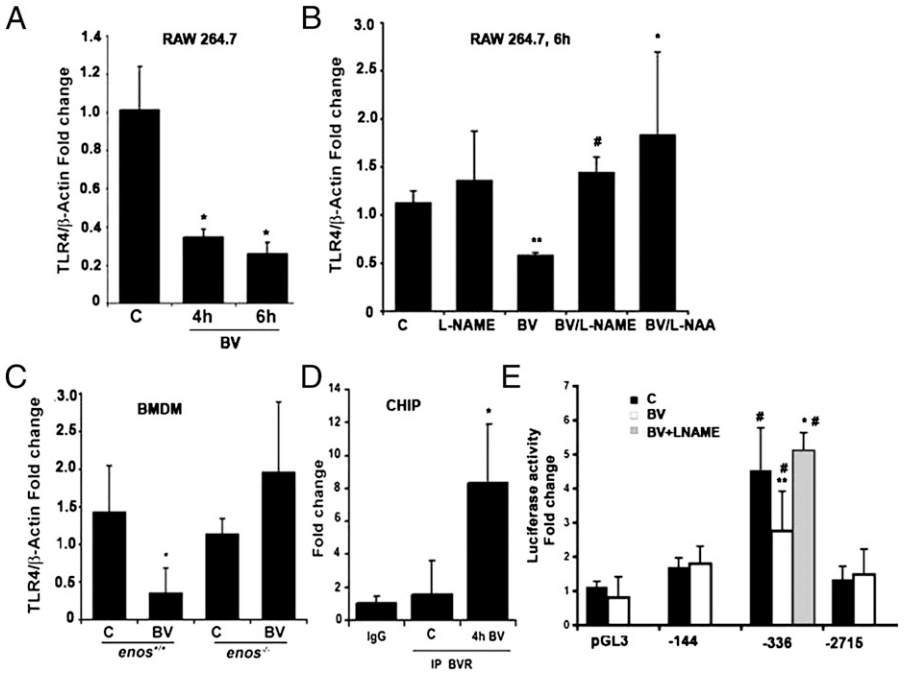

Fig. 4. BV suppresses TLR4 expression dependent on eNOS. (*A–D*) Real-time PCR with primers for TLR4 in RAW 264.7 Mϕ treated with (*A*) BV (50 μM) for 4 and 6 h. **P* < 0.01, BV vs. control (C). (*B*) RAW 264.7 Mϕ pretreated with L-NAME (100 μM) or L-NAA (10 nM) for 1 h before 6 h stimulation with 50 μM BV. ***P* < 0.004 vs. C; #*P* < 0.0004 vs. BV; **P* < 0.04 vs. BV. (*C*) *Enos*$^{+/+}$ and *Enos*$^{-/-}$ bone marrow-derived Mϕ treated with BV for 6 h. **P* < 0.03 vs. control. (*D*) ChIP assay in RAW 264.7 Mϕ treated with BV (50 μM) for 4 h. **P* < 0.02, BV vs. control (C). IgG was used as the negative control. Immunoprecipitation was performed with antibodies to BVR followed by real-time PCR with primers to the TLR4 promoter (−539 to −312 bp). Results represent mean ± SD of three independent experiments repeated in triplicate. (*E*) TLR4 promoter activity was measured in RAW cells that were transfected with the indicated luciferase reporter constructs comprising mutations of the TLR4 gene (27) for 24 h and cultured in the presence (white bars) or absence (black bars) of 50 μM BV for 4 h. L-NAME (100 μM) was applied 1 h before BV. Note that BV blocks luciferase expression in the absence of GATA-4 (−336 bp) but not Ap-1 (−144 bp). Results are presented as fold change over empty vector control and represent mean ± SD of three independent experiments repeated in triplicate. #*P* < 0.001 vs. pGL3; ***P* < 0.001 BV (−336 bp) vs. DMSO (−336 bp); **P* < 0.0008 BV vs. BV + L-NAME.

increase in TNF-α expression in unstimulated and LMP control-transfected Mϕ (Fig. 5*D*). Stimulation of mirBVR or LMP-transduced Mϕ with LPS resulted in additional augmentation of proinflammatory TNF-α levels in mirBVR-transfected RAW 264.7 Mϕ vs. MSCV-LTRmiR30-PIG (LMP) controls (Fig. 5*D*). The heightened TNF-α expression corresponded with low levels of IκB both basally and in the presence of LPS (Fig. 5*E*). After LPS administration, IκB was degraded with expression returning by 1 h in controls as expected. This effect on IκB was absent in mirBVR-transfected RAW 264.7 Mϕ (Fig. 5*E*). Morphologically, mirBVR-transfected RAW 264.7 Mϕ exhibited an activated phenotype vs. LMP controls, which was assessed by the presence of numerous pseudopodia and vacuolization (Fig. 5*F*).

BV Protection Against Acute Hepatitis Requires BVR and eNOS. As previously described, BVR, in addition to cytosolic localization, is also expressed on the surface of hepatocytes as well as residential Mϕ in the liver (Fig. S5*B*). To test the functional importance of a BV-eNOS signaling axis in vivo, we used *Enos*$^{-/-}$- and *Enos*$^{+/+}$-type mice, which were challenged with TNF-α and D-GalN for 6 h. Serum alanine aminotransferases (ALTs) were measured as a marker of liver damage, which in this TNF/D-GalN model, is driven by TNF receptor-mediated hepatocyte necrosis. *Enos*$^{-/-}$ mice showed a partial resistance to the injury, likely caused by other NO-generating compensatory mechanisms (e.g., iNOS, which is known to be protective in this model) (28). BV administration protected *Enos*$^{+/+}$ mice against TNF-α/D-GalN treatment (as previously shown) (5) assessed by serum ALT levels, and the protection afforded by BV was similar in *Enos*$^{-/-}$ mice (Fig. 6*A*).

We posited that constitutive lack of eNOS would result in an increased compensatory role of other NO-generating enzymes in the liver such as iNOS, which has been reported (29–31). We, therefore, used a pharmacologic approach to inhibit NOS activities globally in vivo. BV induced protection against LPS/D-GalN treatment, and the protection afforded by BV against LPS/D-GalN–induced injury was abrogated in animals receiving L-NAME before BV treatment (Fig. 6*B*). The damage in the LPS/D-GalN model is driven by TLR4 on Kupffer cells, which leads to elevated TNF-α expression and hepatocyte death. These data corroborate our in vitro data, showing that the protection provided by BV requires the activity of BVR and eNOS, resulting in decreased TLR4 expression.

Discussion

We present here data explaining the mechanism by which BV, acting through BVR, regulates the inflammatory response by inhibiting TLR4 transcription and protein expression. We show that BVR becomes rapidly S-nitrosylated in response to BV by eNOS-derived NO, leading to translocation of BVR to the nucleus. In the nucleus, BVR binds directly to the TLR4 promoter and represses expression (Fig. S6). Whether it is the plasma membrane BVR isoform or the cytosolic BVR isoform that localizes to the nucleus remains to be determined and is the focus of ongoing studies. Given the potent antiinflammatory effects of BV and BVR as well as HO-1 (5, 6, 32), we posit that this mechanism of TLR4 regulation is innate and used by the cell to quell the inflammatory response after activation and prevent unfettered inflammation after a stimulus, such as bacterial endotoxin. The TLR4 mRNA and protein decrease after LPS stimulation, with a half-life reported to be 60 min, which would coincide with BVR translocation. BVR as a leucine zipper transcription factor interacts with the Ap-1 sites in the promoter regions of HO-1 and ATF-2 (13). BV suppresses TLR4 expression by acting, in part, to direct BVR binding to Ap-1 sites (−144 bp), thereby inactivating proinflammatory mediators, including TLR4 expression in response to inflammatory stimuli (26).

NO signals by posttranslational modification of various proteins, including receptors, enzymes, ion channels, and transcription factors. S-nitrosylation is one form of cysteine modification that alters enzymatic function (e.g., COX2) (33). S-nitrosylation is also well-recognized as a modulator of immune response proteins, including NF-κB and TLR4 (16). BVR was S-nitrosylated in response to LPS and BV, leading us to reason that NO targeting of a cysteine in BVR is critical for nuclear localization of BVR (5). BVR could also potentially be nitrosylated on a tyrosine residue within the tyrosine-methionine-lysine-methionine (YMKM) motif, but this theory was not tested. S-nitrosylation of GAPDH augments binding to Siah1, where nuclear localization signal mediates translocation of GAPDH to the nucleus (34). Perhaps a similar mechanism of NO action on BVR translocation is op-

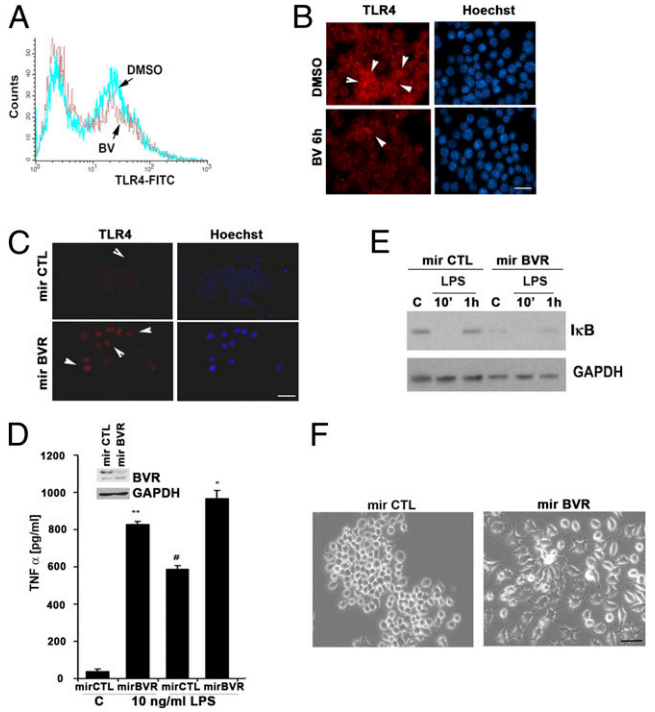

Fig. 5. Lack of BVR leads to a proinflammatory phenotype in Mϕ. (*A*) Flow cytometry of TLR4 FITC levels on the surface of RAW 264.7 Mϕ treated with DMSO or BV (50 μM) for 6 h. Data are representative of at least three independent experiments. (*B* and *C*) Representative immunofluorescence staining of TLR4 in RAW 264.7 Mϕ treated with BV or transfected with mirBVR or mirCTL controls to inhibit expression. Red, TLR4; blue, Hoechst. Images are representative of 10 fields from two independent experiments. Note that BV reduced, whereas blockade of BVR induced TLR4-positive staining. (*D*) ELISA for TNF-α levels in media collected after 24 h from RAW 264.7 Mϕ ± mirBVR knockdown. Data represent mean ± SD of three independent experiments repeated in triplicate. *$P < 0.0001$ mirBVR vs. mirCTL; #$P < 0.001$ mirBVR + LPS vs. mirCTL + LPS; **$P < 0.001$ mirBVR vs. mirCTL. (*Inset*) Immunoblotting with antibody against BVR in cells stably transduced with mirBVR. (*E*) Immunoblot total IκB in mirBVR-expressing RAW 264.7 Mϕ treated ± LPS (100 ng/mL) for 10 min and 1 h. Blot is representative of three independent experiments. (*F*) Morphologic changes in mirBVR-expressing RAW 264.7 Mϕ vs. LMP-transfected control RAW 264.7 Mϕ 24 h after seeding. Note that lack of BVR results in the activation of Mϕ assessed morphologically. Images are representative of 10 fields of view in triplicate.

erational here and highlights an important regulatory process for gene expression.

The role of BV–BVR in modulating NO production and signaling in Mϕ in regulation of the inflammatory response has not been described. We hypothesized that BV through BVR regulates eNOS and NO generation that would, in turn, modify BVR activity as a feedback regulatory mode of action. This hypothesis is strengthened by the fact that BVR_{surf} and eNOS are likely in close proximity with each other in caveolae in the plasma membrane (35). Moreover, it is feasible that, given the potent antiinflammatory effects of BV and BVR in models of sepsis, vascular trauma, and ischemia reperfusion injury (5, 6), modification of BVR by NO is available and thus, a plausible molecular mechanism to reestablish homeostasis and the overall cellular response to exaggerated oxidative stress.

The expression of eNOS in primary Mϕ and RAW 264.7 Mϕ is apparent (20) (Fig. 1), and eNOS is the likely source of NO: iNOS was not induced after BV stimulation, and the data do not fit the kinetic of iNOS expression in Mϕ treated with LPS. BVR-induced phosphorylation of eNOS is dependent, in part, on intracellular levels of calcium and CaMKK in endothelial cells (36, 37). The role of CaMKK in eNOS regulation, however, has not been reported in Mϕ, and therefore, the data presented here also describe the link made between these two enzymes, because BV induced a rapid and transient calcium influx in Mϕ that precedes eNOS phosphorylation.

In summary, we have identified a mechanism by which BV/BVR imparts salutary effects in models of acute inflammation. We describe transcriptional repressor activity for BVR acting to block additional TLR4 expression. Our in vitro findings translated in vivo, where we observed that BV protected against both TNF-α– and LPS-mediated liver damage, likely through modulating the inflammatory response driven by Kupffer cells that are known to direct a potent inflammatory response that amplifies hepatocyte cell death (5, 6). Pharmacological blockade of NO generation partly abrogated the protective effects ascribed to BV in models of acute liver damage in rats (5, 6). The fact that blockade of NOS did not amplify the liver injury is likely explained, in part, by multiple signaling redundancies that could be targeted by BV and involvement of multiple cell types in the liver, including hepatocytes and stellate cells. BV has known antiapoptotic effects, and it protects the liver from ischemia reperfusion injury involving JNK MAPK and modulation of cytokine production, including regulation of IL-10 by BVR in response to endotoxin (5, 38, 39).

Collectively, we identify BVR as a target for NO-dependent S-nitrosylation and elucidate mechanisms by which BVR translocates to the nucleus to repress TLR4 expression. We postulate that BV-induced activation of eNOS in Mϕ and likely endothelial cells is a critical regulatory mechanism for an appropriate and controlled inflammatory response.

Materials and Methods

Animal Treatment. C57BL6/J WT (*Enos*$^{+/+}$) and *Enos*$^{-/-}$ mice were purchased from Jackson Laboratories. All animals were held under Specific Pathogen Free (SPF) conditions, and the experiments were approved by the Beth Israel Deaconess Medical Center Animal Care and Use Committee. BV was freshly

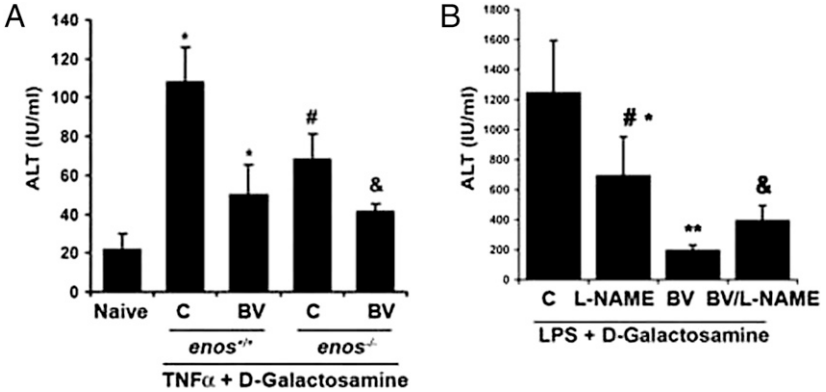

Fig. 6. BV blocks acute liver damage in vivo dependent on NO. (*A*) Serum transaminase levels measured in *Enos*$^{-/-}$ and *Enos*$^{+/+}$ mice 6 h after TNF-α+ D-GalN in the presence and absence of BV (35 mg/kg i.p.) or saline as control administered 1 h before TNF–D-GalN. Results represent mean ± SD of six to eight mice per group. Kruskal–Wallis test for multiple comparisons: $P = 0.015$; *$P < 0.05$ BV vs. C or C vs. naïve; #$P < 0.05$ *Enos*$^{-/-}$ vs. *Enos*$^{+/+}$; &$P < 0.02$ BV, *Enos*$^{-/-}$ vs. C, *Enos*$^{-/-}$. (*B*) Mice were administered BV or saline as above ± 30-min pretreatment with L-NAME (20 mg/kg i.p.) and then followed by injection of LPS + D-GalN. Serum transaminases (ALT) were measured at 6 h. Results represent mean ± SD of four to six mice per group. Kruskal–Wallis test for multiple comparisons: **$P < 0.0.0005$ vs. C; *$P < 0.002$ BV/LPS vs. BV/L-NAME/LPS; #$P < 0.003$ BV/LPS vs. L-NAME/LPS; & $P < 0.002$ BV/L-NAME/LPS vs. LPS.

PHYSIOLOGY

dissolved in 0.2 N NaOH, adjusted to a final pH of 7.4 with HCl, and kept in the dark. L-NAME at the dose of 20 mg/kg was applied 30 min before BV treatment. BV (35 mg/kg i.p.) was administered to mice 16 h and again, 2 h before LPS/D-GalN (250 μg/kg i.p. and 750 mg/kg i.p., *Escherichia coli* serotype 0127:08; Sigma). The serum samples for ALT measurement were harvested 6 h after LPS/D-GalN treatment (n = 6 mice/group).

NO Generation Measurement. NO generation was measured in a sealed vessel in which the solution and head space were purged with helium. The vessel was connected in line with a Nitric Oxide Analyzer (Sievers Co.) as previously described. In some conditions, RAW 264.7 cells were pretreated with L-NIO (100 μM). Cells were treated with LPS (100 ng/mL) or BV (50 μM). NO generation was normalized to r-cell protein concentration as measured by the BCA Protein Assay Kit (Pierce).

Cell Fractionation. Cytosolic and membrane cell fractions were isolated using the manufacturer's protocol for the Plasma Membrane Protein Extraction Kit (BioVision). Protein extracts were subjected to additional analyses by immunoblotting and immunoprecipitation as previously described (5, 29). Nuclear extraction was performed using the manufacturer's protocol (Pierce or BioVision).

ChIP Assay, RNA Isolation, and Real-Time PCR. ChIP assay was performed as previously described (27) using the primers for the first part of the TLR4 promoter (30). RNA isolation and real-time PCR were performed as previously described (27). The following primers were used: TLR4 F: 5′CTGGTTGCAGAAAATGCCAG3′ and TLR4 R: 5′CTGGATAAATCCAGCCACTG3′. β-actin primers were previously described (31).

Immunoblotting, Immunoprecipitation, and S-Nitrosylation Assay. Snap-frozen tissue samples were homogenized in ice-cold tissue lysis buffer (250 mM NaCl, 5 mM EDTA, 1% Triton X-100, 10 mM Tris·HCl, pH 7.5) containing the protease inhibitor mixture Complete Mini (Roche). For coimmunoprecipitation, 100–500 μg protein lysates in RIPA buffer and the protease inhibitor mixture were mixed with appropriate antibodies and 30 μL Protein A/G Plus agarose beads (Santa Cruz Biotechnology) and then rocked for 2.5 h at 4 °C. The proteins were washed with RIPA buffer and eluted (at 95 °C for 5 min in SDS loading buffer). Immunoblotting was performed as previously described (40). S-nitrosylation assay was performed using the manufacturer's protocol for the S-Nitrosylation Kit (Cayman Chemical).

Calcium Flux Measurement. Rhod-X (Molecular Probes; Invitrogen) was used as an indicator of calcium influx using the manufacturer's protocol. Time-lapse imaging was performed using an Axiovert Zeiss Microscope.

BVR Activity. BVR activity was measured as previously described (5). The lysates of cytoplasmic and nuclear fractions were isolated as described above and used in the assay.

ELISA. TNF-α ELISA was from R&D Systems and was used according to the manufacturer's protocol.

Statistical Analysis. Results are presented as the mean ± SD. Statistical comparison was performed by use of student t test, one- or two-way ANOVA (posthoc Tukey test), or nonparametric Wilcoxon or Kruskal–Wallis test (SPSS Inc). $P < 0.05$ was considered to be statistically significant.

ACKNOWLEDGMENTS. We thank Piotr Kaczmarek for the creative graphic design and the Julie Henry Fund at the Transplant Institute of the Beth Israel Deaconess Medical Center for continued support. This work was supported in part by American Heart Association Grant 10SDG2640091 (to B.W.) and National Institutes of Health Grant R01GM088666-01 (to L.E.O.).

1. Lerner-Marmarosh N, Miralem T, Gibbs PE, Maines MD (2008) Human biliverdin reductase is an ERK activator; hBVR is an ERK nuclear transporter and is required for MAPK signaling. *Proc Natl Acad Sci USA* 105:6870–6875.
2. Maines MD (2005) New insights into biliverdin reductase functions: Linking heme metabolism to cell signaling. *Physiology (Bethesda)* 20:382–389.
3. Kapitulnik J, Maines MD (2009) Pleiotropic functions of biliverdin reductase: Cellular signaling and generation of cytoprotective and cytotoxic bilirubin. *Trends Pharmacol Sci* 30:129–137.
4. Lerner-Marmarosh N, et al. (2005) Human biliverdin reductase: A member of the insulin receptor substrate family with serine/threonine/tyrosine kinase activity. *Proc Natl Acad Sci USA* 102:7109–7114.
5. Wegiel B, et al. (2009) Cell surface biliverdin reductase mediates biliverdin-induced anti-inflammatory effects via phosphatidylinositol 3-kinase and Akt. *J Biol Chem* 284: 21369–21378.
6. Sarady-Andrews JK, et al. (2005) Biliverdin administration protects against endotoxin-induced acute lung injury in rats. *Am J Physiol Lung Cell Mol Physiol* 289:L1131–L1137.
7. Maines MD (2010) Potential application of biliverdin reductase and its fragments to modulate insulin/IGF-1/MAPK/PI3-K signaling pathways in therapeutic settings. *Curr Drug Targets* 11:1586–1594.
8. Greenberg AJ, Bossenmaier I, Schwartz S (1971) Green jaundice. A study of serum biliverdin, mesobiliverdin and other green pigments. *Am J Dig Dis* 16:873–880.
9. Greenberg DA (2002) The jaundice of the cell. *Proc Natl Acad Sci USA* 99:15837–15839.
10. Bach FH (2006) Heme oxygenase-1 and transplantation tolerance. *Hum Immunol* 67:430–432.
11. Cowger ML (1971) Mechanism of bilirubin toxicity on tissue culture cells: Factors that affect toxicity, reversibility by albumin, and comparison with other respiratory poisons and surfactants. *Biochem Med* 5:1–16.
12. Maines MD (2007) Biliverdin reductase: PKC interaction at the cross-talk of MAPK and PI3K signaling pathways. *Antioxid Redox Signal* 9:2187–2195.
13. Ahmad Z, Salim M, Maines MD (2002) Human biliverdin reductase is a leucine zipper-like DNA-binding protein and functions in transcriptional activation of heme oxygenase-1 by oxidative stress. *J Biol Chem* 277:9226–9232.
14. Maines MD, Ewing JF, Huang TJ, Panahian N (2001) Nuclear localization of biliverdin reductase in the rat kidney: Response to nephrotoxins that induce heme oxygenase-1. *J Pharmacol Exp Ther* 296:1091–1097.
15. Mancuso C, et al. (2008) Bilirubin as an endogenous modulator of neurotrophin redox signaling. *J Neurosci Res* 86:2235–2249.
16. Into T, et al. (2008) Regulation of MyD88-dependent signaling events by S nitrosylation retards toll-like receptor signal transduction and initiation of acute-phase immune responses. *Mol Cell Biol* 28:1338–1347.
17. Wu HS, et al. (2005) Effect of nitric oxide on toll-like receptor 2 and 4 gene expression in rats with acute lung injury complicated by acute hemorrhage necrotizing pancreatitis. *Hepatobiliary Pancreat Dis Int* 4:609–613.
18. Kim YM, et al. (2000) Nitric oxide prevents tumor necrosis factor alpha-induced rat hepatocyte apoptosis by the interruption of mitochondrial apoptotic signaling through S-nitrosylation of caspase-8. *Hepatology* 32:770–778.
19. Dimmeler S, et al. (1999) Activation of nitric oxide synthase in endothelial cells by Akt-dependent phosphorylation. *Nature* 399:601–605.
20. Connelly L, Jacobs AT, Palacios-Callender M, Moncada S, Hobbs AJ (2003) Macrophage endothelial nitric-oxide synthase autoregulates cellular activation and pro-inflammatory protein expression. *J Biol Chem* 278:26480–26487.
21. Baranano DE, Rao M, Ferris CD, Snyder SH (2002) Biliverdin reductase: A major physiologic cytoprotectant. *Proc Natl Acad Sci USA* 99:16093–16098.
22. Sedlak TW, Snyder SH (2004) Bilirubin benefits: Cellular protection by a biliverdin reductase antioxidant cycle. *Pediatrics* 113:1776–1782.
23. Sedlak TW, et al. (2009) Bilirubin and glutathione have complementary antioxidant and cytoprotective roles. *Proc Natl Acad Sci USA* 106:5171–5176.
24. Pereira PJ, et al. (2001) Structure of human biliverdin IXbeta reductase, an earl fetal bilirubin IXbeta producing enzyme. *Nat Struct Biol* 8:215–220.
25. Uehara T, et al. (2006) S-nitrosylated protein-disulphide isomerase links protein misfolding to neurodegeneration. *Nature* 441:513–517.
26. Roger T, et al. (2005) Critical role for Ets, AP-1 and GATA-like transcription factors in regulating mouse Toll-like receptor 4 (Tlr4) gene expression. *Biochem J* 387:355–365.
27. Wegiel B, et al. (2008) Multiple cellular mechanisms related to cyclin A1 in prostate cancer invasion and metastasis. *J Natl Cancer Inst* 100:1022–1036.
28. Zuckerbraun BS, et al. (2003) Carbon monoxide protects against liver failure through nitric oxide-induced heme oxygenase 1. *J Exp Med* 198:1707–1716.
29. Kutty RK, Maines MD (1981) Purification and characterization of biliverdin reductase from rat liver. *J Biol Chem* 256:3956–3962.
30. Zampetaki A, Xiao Q, Zeng L, Hu Y, Xu Q (2006) TLR4 expression in mouse embryonic stem cells and in stem cell-derived vascular cells is regulated by epigenetic modifications. *Biochem Biophys Res Commun* 347:89–99.
31. Bilban M, et al. (2006) Carbon monoxide orchestrates a protective response through PPARgamma. *Immunity* 24:601–610.
32. Otterbein LE, Soares MP, Yamashita K, Bach FH (2003) Heme oxygenase-1: Unleashing the protective properties of heme. *Trends Immunol* 24:449–455.
33. Sun J, Steenbergen C, Murphy E (2006) S-nitrosylation: NO-related redox signaling to protect against oxidative stress. *Antioxid Redox Signal* 8:1693–1705.
34. Hara MR, et al. (2005) S-nitrosylated GAPDH initiates apoptotic cell death by nuclear translocation following Siah1 binding. *Nat Cell Biol* 7:665–674.
35. Kim HP, Wang X, Galbiati F, Ryter SW, Choi AM (2004) Caveolae compartmentalization of heme oxygenase-1 in endothelial cells. *FASEB J* 18:1080–1089.
36. Schneider JC, et al. (2003) Involvement of Ca2+/calmodulin-dependent protein kinase II in endothelial NO production and endothelium-dependent relaxation. *Am J Physiol Heart Circ Physiol* 284:H2311–H2319.
37. Bredt DS, Ferris CD, Snyder SH (1992) Nitric oxide synthase regulatory sites. Phosphorylation by cyclic AMP-dependent protein kinase, protein kinase C, and calcium/calmodulin protein kinase; identification of flavin and calmodulin binding sites. *J Biol Chem* 267:10976–10981.
38. Fondevila C, et al. (2003) Biliverdin protects rat livers from ischemia/reperfusion injury. *Transplant Proc* 35:1798–1799.
39. Tang LM, et al. (2007) Exogenous biliverdin ameliorates ischemia-reperfusion injury in small-for-size rat liver grafts. *Transplant Proc* 39:1338–1344.
40. Chin BY, et al. (2007) Hypoxia-inducible factor 1alpha stabilization by carbon monoxide results in cytoprotective preconditioning. *Proc Natl Acad Sci USA* 104:5109–5114.